

A simple and effective inverse projection scheme for void distribution control in topology optimization

S. R. M. Almeida · G. H. Paulino · E. C. N. Silva

Received: 6 January 2008 / Revised: 29 July 2008 / Accepted: 15 October 2008 / Published online: 8 January 2009
© Springer-Verlag 2008

Abstract The ability to control both the minimum size of holes and the minimum size of structural members are essential requirements in the topology optimization design process for manufacturing. This paper addresses both requirements by means of a unified approach involving mesh-independent projection techniques. An inverse projection is developed to control the minimum hole size while a standard direct projection scheme is used to control the minimum length of structural members. In addition, a heuristic scheme combining both contrasting requirements simultaneously is discussed. Two topology optimization implementations are contributed: one in which the projection (either inverse or direct) is used at each iteration; and the other in which a two-phase scheme is explored. In the first phase, the compliance minimization is carried out without any projection until convergence. In the

second phase, the chosen projection scheme is applied iteratively until a solution is obtained while satisfying either the minimum member size or minimum hole size. Examples demonstrate the various features of the projection-based techniques presented.

Keywords Topology optimization · Projection functions · Direct projection · Inverse projection · Combined projection · Two-phase optimization

1 Introduction

Engineers aim at improving the structural optimization process in order to find an efficient answer to the problem of automatic design of structural components. Although optimization techniques can play a role in several stages of the design process, the state-of-the-art does not allow a complete automation yet. Some techniques, such as parameter optimization, are more suited to the final stages of the design process because they can easily incorporate limit state constraints (e.g. Nitsopoulos and Lauber 2007). On the other hand, topology optimization including material distribution fits better in the initial stages of the design process. Topology optimization is of considerable practical importance because it can lead to savings and design improvements (Rozvany 2001a). Since the development of the SIMP (Solid Isotropic Material with Penalization) method (e.g. Zhou and Rozvany 1991), which was previously developed under different terminology, such as the “direct approach” or “artificial density approach” by Bendsoe (1989), the range of applications of

S. R. M. Almeida
Escola de Engenharia Civil, Universidade Federal de Goiás,
Av. Universitária, 1488, Qd. 86, Setor Universitário,
Goiânia, GO, 74605-220, Brazil
e-mail: sylvia@eec.ufg.br

G. H. Paulino (✉)
Department of Civil and Environmental Engineering,
University of Illinois at Urbana-Champaign,
Newmark Laboratory, 205 North Mathews Avenue,
Urbana, IL 61801, USA
e-mail: paulino@uiuc.edu

E. C. N. Silva
Department of Mechatronics and
Mechanical Systems Engineering,
Escola Politécnica da Universidade de São Paulo,
Av. Professor Mello Moraes, 2231, São Paulo,
SP, 05508-900, Brazil
e-mail: ecnsilva@usp.br

topology optimization has increased steadily (Rozvany 2001b).

Achieving control of manufacturing design and considering limit state constraints are some of the most important issues to move topology optimization beyond a preliminary design tool. Control of structural member sizes and minimum sizes of holes are just two of several manufacturing requirements that must be observed in the design process. Features such as axial and radial symmetry, extrusion (see Ishii and Aomura 2004), casting and machining (see Chang and Tang 2001 and Zuo et al. 2006) are relevant to topology optimization and contribute to extend the role played by these techniques in the design process.

Techniques to avoid numerical instabilities in the topology optimization process also provide an indirect control over the resulting structural member sizes. For instance, the weighted average over element densities adopted in most density filters (Bourdin 2001; Guo and Gu 2004; Wang and Wang 2005) and the weighted average over sensitivities adopted in the sensitivity filters (Sigmund 1997, 2001 and Borrvall and Petersson 2001) augment the structural member size as the characteristic dimension of the filter is increased. A mesh-independent projection scheme to achieve minimum length scale on structural members obtained by means of topology optimization using compliance minimization has been presented by Guest et al. (2004). This scheme has been extended beyond compliance minimization by Carbonari et al. (2007, 2009) in a multi-physics setting.

This paper addresses the problem of imposing minimum size of holes as well as minimum length scale to structural members (Fig. 1). We propose an inverse projection scheme to enforce the minimum size of holes. We also propose a heuristic combination of this scheme with a direct projection scheme to achieve

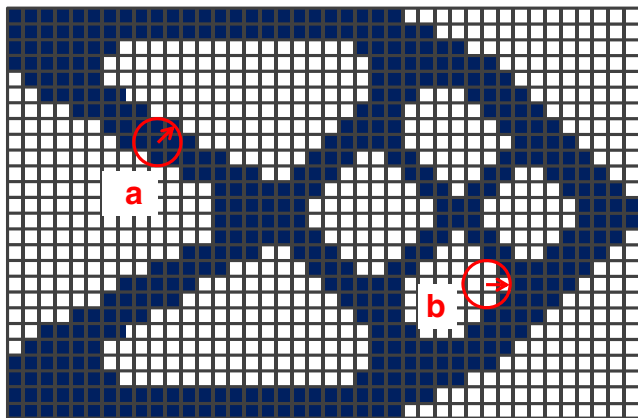


Fig. 1 Length scale associated to **a** solid member and **b** hole sizes

minimum member size control. The schemes are combined without any additional constraints, filters or penalty functions. Notice that all the projection schemes (direct, inverse and combined) only encourage limitation of minimum feature size but do not impose constraints in a strict sense.

Recently, Sigmund (2007) introduced the use of morphology-based operators to control the size of members and holes. The inverse scheme approach has some similarities with the morphology operators “erode” and “open”. Both methods aim to control the size of the holes. However, the control provided by those morphology operators does not offer a direct relation between the operator parameter and the size of the holes as it is done in the present inverse scheme, and does not suggest any scheme to combine the operators as well.

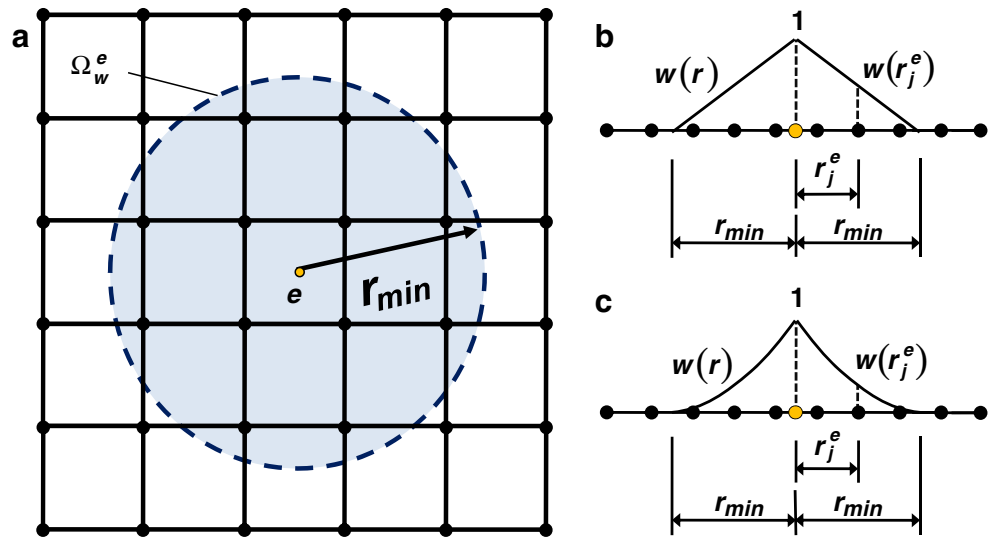
The remainder of this paper is organized as follows. Section 2 presents the direct projection scheme, Section 3 introduces the inverse projection scheme, and Section 4 presents a possible alternative to combine both schemes. Section 5 provides information on the topology optimization formulation, together with some details of the implementation including evaluation of sensitivities. Section 6 contributes an alternative computational implementation involving a two-phase topology optimization scheme, which is explored in two sequential phases. Several examples and numerical results are provided in Section 7. The conclusions are given in Section 8.

2 Direct projection

Projection schemes are used in topology optimization to project nodal values onto an element space (to be used in the finite element analysis). Some of these functions such as the shape functions used in the continuous approximation of material distribution (CAMD) technique (Matsui and Terada 2004) are mesh-dependent. Because each function influences only the elements connected to the related node, the region of the domain under its influence becomes smaller as the mesh is refined. Mesh-independent schemes can be achieved with mesh-independent projection regions, as discussed below. In general, techniques used to achieve mesh independent solutions also tend to alleviate the checkerboard problem (Zhou et al. 2001).

Guest et al. (2004) proposed a mesh-independent projection scheme to achieve minimum length scale on structural members generated by topology optimization. The nodes inside a circular region Ω_w^e in the neighborhood of the element of reference are included

Fig. 2 Direct projection scheme: **a** domain Ω_w^e , **b** linear weight function, **c** parabolic weight function



in the evaluation of the element density ρ^e used in the finite element analysis (Fig. 2a). The set of nodes S_w^e to be projected are defined by

$$\mathbf{x}_j \in S_w^e \quad \text{if} \quad r_j^e = |\mathbf{x}_j - \mathbf{x}^e| \leq r_{\min} \quad (1)$$

where \mathbf{x}_j are the coordinates of the node j , \mathbf{x}^e are the coordinates of the center of the element, and r_j^e is the distance between the center of the element e and the node j . The projection consists essentially of a cone of base $2 r_{\min}$ and unit height centered at the center of the element such that

$$\rho^e = \frac{\sum_{j \in S_w^e} y_j w(\mathbf{x}_j - \mathbf{x}^e)}{\sum_{j \in S_w^e} w(\mathbf{x}_j - \mathbf{x}^e)} \quad (2)$$

$$w(\mathbf{x}_j - \mathbf{x}^e) = \begin{cases} \frac{r_{\min} - r_j^e}{r_{\min}} & \text{if } x_j \in \Omega_w^e \\ 0 & \text{if } x_j \notin \Omega_w^e \end{cases} \quad (3)$$

The nodal variables y_j are weighted to evaluate the element volume fraction ρ^e of element e , as shown in (2), using the linear weight function defined in (3) and shown in Fig. 2b. Other functions can be used as well.

The weight function (3) is mesh-independent because r_{\min} is an invariant length scale, however, the number of nodes evaluated in the weight function increases as the mesh is refined. The radius r_{\min} is a physical length scale, which imposes that the minimum allowable member size corresponds to $2 r_{\min}$, the basis of the projection cone.

Regarding projection schemes, a multiple choice approach may be advantageous in some instances, e.g. to reduce regions with intermediate densities at the

borders of the structural elements. Thus, an alternative parabolic weight function is proposed according to

$$w(\mathbf{x}_j - \mathbf{x}^e) = \begin{cases} \left(\frac{r_{\min} - r_j^e}{r_{\min}} \right)^2 & \text{if } x_j \in \Omega_w^e \\ 0 & \text{if } x_j \notin \Omega_w^e \end{cases} \quad (4)$$

as illustrated in Fig. 2c.

3 Inverse projection scheme

A unified approach involving mesh independent projection techniques is employed to enforce the minimum size of holes in topology optimization by means of inverse projections. The inverse projection scheme is defined in a circular region Ω_{inv}^e in the neighborhood of the element (Fig. 3a). The set nodes S_{inv}^e in the Ω_{inv}^e region are defined by

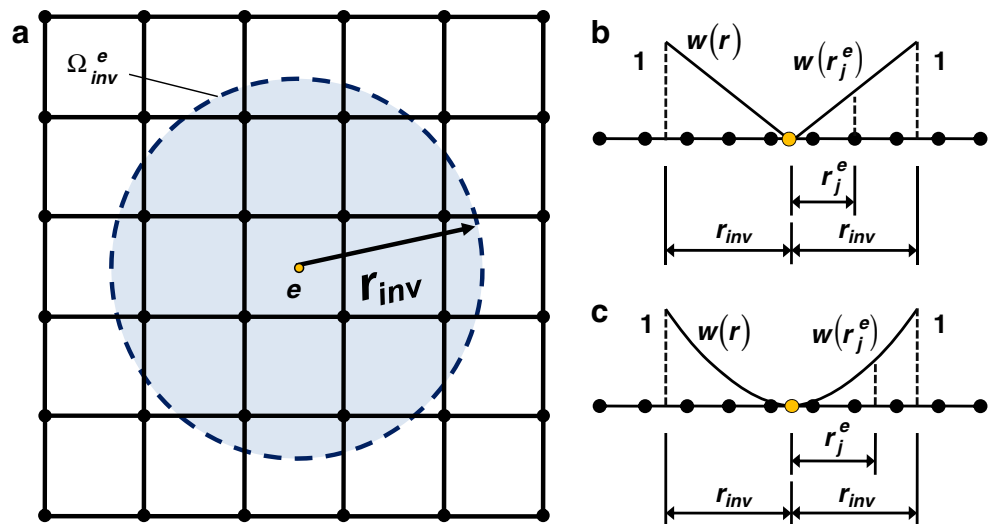
$$\mathbf{x}_j \in S_{\text{inv}}^e \quad \text{if} \quad r_j^e = |\mathbf{x}_j - \mathbf{x}^e| \leq r_{\text{inv}} \quad (5)$$

The inverse projection scheme consists essentially of an inverse cone of base $2 r_{\text{inv}}$ and unit height centered on the circle of radius r_{inv} . Moreover,

$$\rho^e = \frac{\sum_{j \in S_{\text{inv}}^e} y_j w_{\text{inv}}(\mathbf{x}_j - \mathbf{x}^e)}{\sum_{j \in S_{\text{inv}}^e} w_{\text{inv}}(\mathbf{x}_j - \mathbf{x}^e)} \quad (6)$$

Below we present the development for the inverse projections which are linear and parabolic, respectively. Other projection functions can be developed as well.

Fig. 3 Inverse projection scheme: **a** domain Ω_{inv}^e , **b** linear weight function, **c** parabolic weight function



3.1 Inverse linear projection

The weight for the inverse linear projection is given by

$$w_{inv}(\mathbf{x}_j - \mathbf{x}^e) = \begin{cases} \frac{r_j^e}{r_{inv}} & \text{if } x_j \in \Omega_{inv}^e \\ 0 & \text{if } x_j \notin \Omega_{inv}^e \end{cases} \quad (7)$$

The nodes in the region Ω_{inv}^e are weighted proportionally to the distance between the node and the center of the element, as shown in (7) and in Fig. 3b, and the element volume fraction ρ^e of element e is evaluated using the nodal variables y_j as shown in (6). The radius r_{inv} indicates that the minimum allowable length scale for any hole corresponds to $2 r_{inv}$, the basis of the inverse projection cone.

3.2 Inverse quadratic projection

The alternative parabolic inverse weight function is given by:

$$w_{inv}(\mathbf{x}_j - \mathbf{x}^e) = \begin{cases} \left(\frac{r_j^e}{r_{inv}}\right)^2 & \text{if } x_j \in \Omega_{inv}^e \\ 0 & \text{if } x_j \notin \Omega_{inv}^e \end{cases} \quad (8)$$

as illustrated by Fig. 3c. This projection, as well as the projections given above (both inverse and direct), are investigated further by means of numerical examples.

4 Discussion on a combined projection scheme

An important feature concerning topology optimization design consists of imposing a minimum length scale to structural elements, while at the same time ensuring that the optimization process does not generate

very small holes which are difficult to manufacture. The projection function (2) solves the minimum length scale problem and the projection function (6) solves the minimum hole size problem. Both of them can be easily implemented. Imposing the two conditions together requires additional considerations because the two functions are conflicting.

We propose an empirical approach, which consists of choosing between the direct and the inverse scheme “on the fly” based on the actual volume of voids surrounding the element. An element placed in a region of high element density (Fig. 4a) is considered to be part of a structural member and, therefore, the direct projection scheme is applied to guarantee the minimum member size. If, on the other hand, the element is placed on a low element density region (Fig. 4b), it is considered to be predominantly part of a hole region and, therefore, the inverse projection scheme is applied to enforce a minimum size for the hole.

The combined scheme follows the unified approach predominant in the paper. The projection assessment is

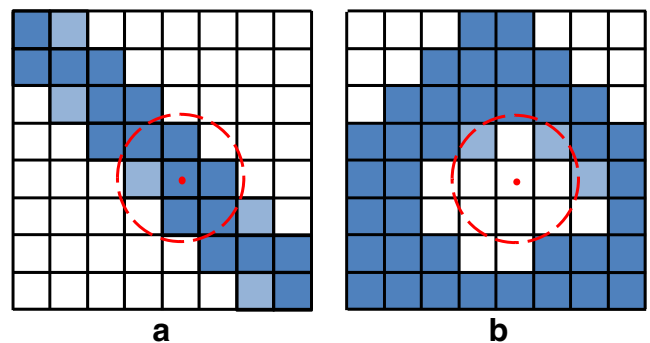


Fig. 4 Use of **a** direct projection and **b** inverse projection

carried out in a circular region Ω_c of radius r_c centered at the center of element e . The set of nodes S_c^e in the Ω_c^e region are defined by

$$\mathbf{x}_j \in S_c^e \quad \text{if} \quad r_j^e = |\mathbf{x}_j - \mathbf{x}^e| \leq r_c \quad (9)$$

The volume of voids V_v^e in Ω_c^e is computed as,

$$V_v^e(\mathbf{y}) = \sum_{j \in \Omega_c^e} v_j (1 - \rho^e(y_j) + y_{\min})^\eta \quad (10)$$

where v_j is the volume of the element j , and \mathbf{y} is the vector of the nodal densities in Ω_c^e . The power index η was introduced (Guest 2009) in order to penalize the contribution of the intermediate volume fraction (adopting $\eta \geq 1$). For large values of η only elements whose volume fractions achieve the lower bound y_{\min} are counted towards the total volume of voids. The actual percentage of voids surrounding element e is then obtained by normalizing the actual volume of voids (10), i.e.

$$c_v^e(\mathbf{y}) = \frac{V_v^e(\mathbf{y})}{\sum_{i \in \Omega_c^e} v_i} \quad (11)$$

The actual percentage of voids c_v^e (11) is employed to select the projection scheme to be applied to evaluate the element volume fraction ρ^e used in the finite element analysis. The choice depends on an empirical limit change factor c_c defined by the designer. The inequality $c_v^e < c_c$ indicates that the element is in a solid structural member region (Fig. 4a), and, therefore, the projection scheme (2), together with either the weight function (3) or (4), shall be applied; while $c_v^e \geq c_c$ indicates that the element is in a hole region (Fig. 4b) and, therefore, the projection scheme (6), together with either the weight function (7) or (8), shall be applied.

Some remarks concerning the combined projection scheme follow. The scheme identifies three regions: (1) region Ω_c^e , where the actual percentage of voids is computed in order to select the proper projection scheme; (2) region Ω_{inv}^e , related to the minimum size of the holes; and (3) region Ω_w^e , related to the minimum length scale of structural members. The first two are related to the volume of voids surrounding an element and, for simplicity, we assume that both are the same region. Thus, we employ the radius r_c (which defines the region Ω_c^e where the actual percentage of voids is computed) to be equal to r_{inv} (which defines the region Ω_{inv}^e associated to the minimum size of the holes). The regions (Ω_w^e , Ω_{inv}^e and Ω_c^e) do not change during the optimization process and, thus, are determined at the beginning of the computations.

We also call attention to the fact that elements placed very close to the structural members, but still

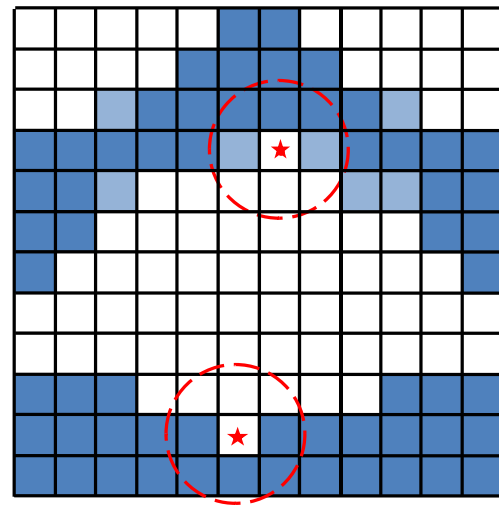


Fig. 5 Elements in which the use of the direct projection scheme is suitable

in the “hole region”, as the elements neighboring the stair-type region in Fig. 5, have intermediate values of c_v^e . Although these are low density elements, they must be gathered to the structural member region (by increasing their densities to enforce the minimum member size) and not gathered to the void region. Thus, the limit change factor c_c must be carefully chosen. In general, we recommend c_c to be taken between 0.6 and 0.8.

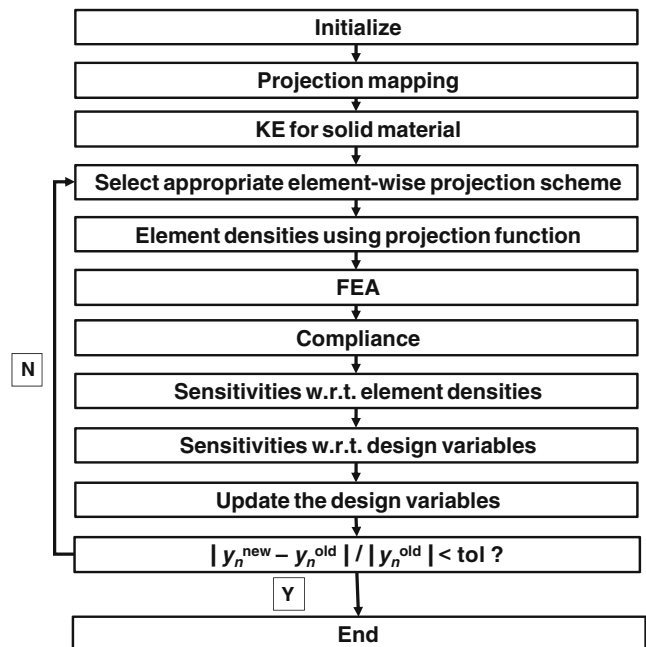
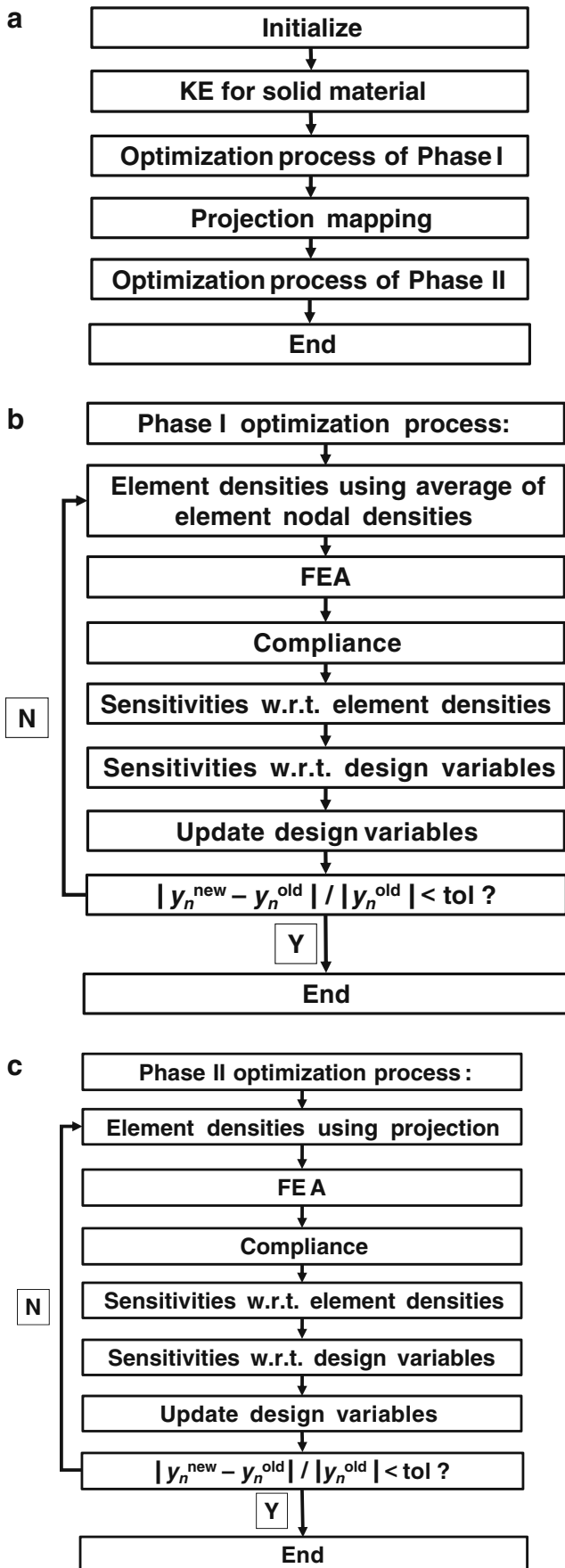


Fig. 6 Topology optimization scheme for the single phase (standard) algorithm



◀ **Fig. 7** Two-phase topology optimization: **a** main algorithm, **b** Phase I algorithm, **c** Phase II algorithm

5 Basic formulation and implementation

Topology design optimization is traditionally formulated as a material distribution problem in which solid material and void regions are represented by discrete density values 1 and 0, respectively. The SIMP model (e.g. Bendsoe 1989; Zhou and Rozvany 1991) relaxes the formulation considering a continuous variation of density in the interval $[\rho_{min}, 1]$ and makes material properties continuously dependent on the local amount of material. A power-law relation is used to penalize intermediate densities and recover the discrete nature of the final solution. At any point of the design domain Ω :

$$E^H(\mathbf{x}) = E_s \rho(\mathbf{x})^p, \quad p > 1 \tag{12}$$

where \mathbf{x} denotes the coordinates of the point; $E^H(\mathbf{x})$ the Young’s modulus at coordinates \mathbf{x} ; $\rho(\mathbf{x})$ the pseudo densities at coordinates \mathbf{x} ; E_s the Young’s modulus of the solid material; and p the penalization factor.

The performance of the proposed projection schemes (inverse, direct and combined) is assessed through computational implementation of the minimum compliance using the SIMP model (12). It can be solved using, for example, the optimality criteria:

$$\begin{aligned} \min \quad & C(\mathbf{y}, \mathbf{U}) = \mathbf{U}^T \mathbf{K} \mathbf{U} \\ \text{s.t.} \quad & V(\mathbf{y}) = \sum y_j \leq f V_0 \\ & y_{min} \leq y_j \leq 1 \end{aligned} \tag{13}$$

The objective function is the compliance of the structure $C(\mathbf{y}, \mathbf{U})$; \mathbf{U} is the global displacement vector, which depends on the design variables \mathbf{y} ; \mathbf{K} is the global

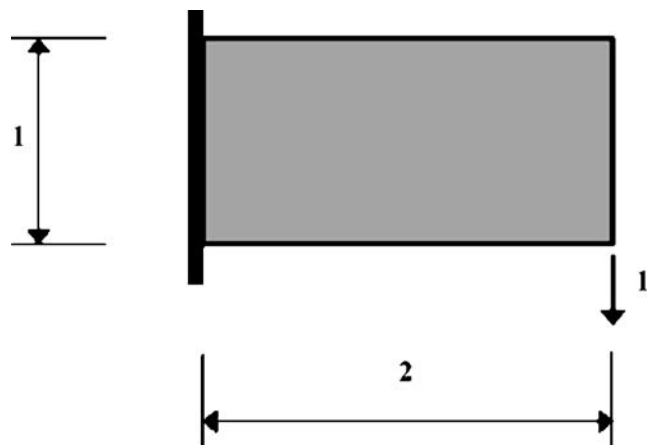


Fig. 8 Cantilever beam

Fig. 9 Topology of the cantilever beam obtained using linear projection and mesh discretization 100×50 : **a** $r_{\min} = 2$ elements **b** $r_{\text{inv}} = 2$ elements. Note: the *white bar at the top right* illustrates the length-scale of the projection ($d = 2r$)

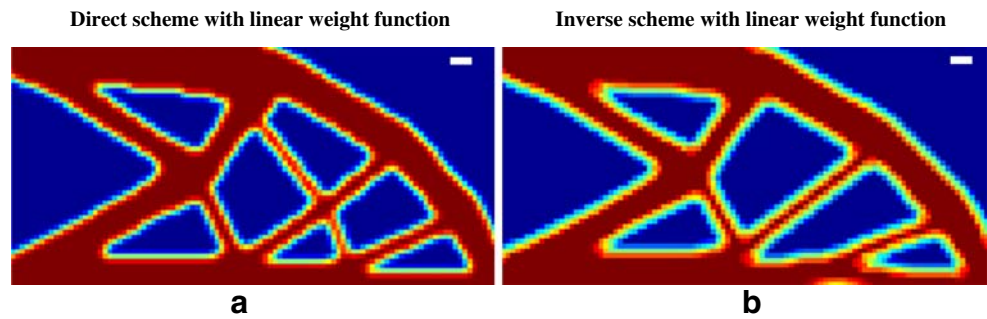


Fig. 10 Topology of the cantilever beam obtained using parabolic projection and mesh discretization 100×50 : **a** $r_{\min} = 2$ elements, **b** $r_{\text{inv}} = 2$ elements, **c** $r_{\min} = 3$ elements, **d** $r_{\text{inv}} = 3$ elements, **e** $r_{\min} = 4$ elements, **f** $r_{\text{inv}} = 4$ elements. Note: The *white bar at the top right* illustrates the length-scale of the projection ($d = 2r$)

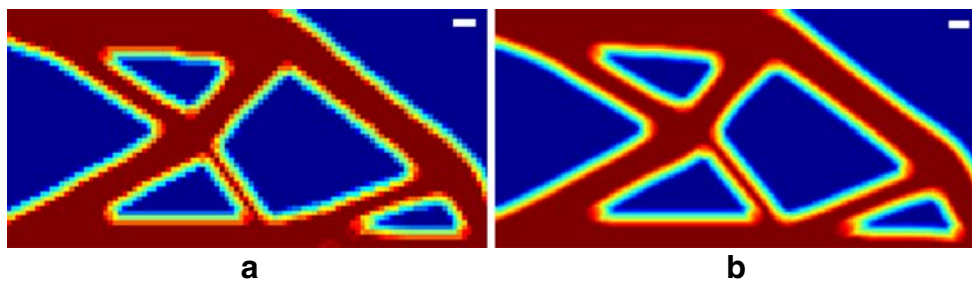
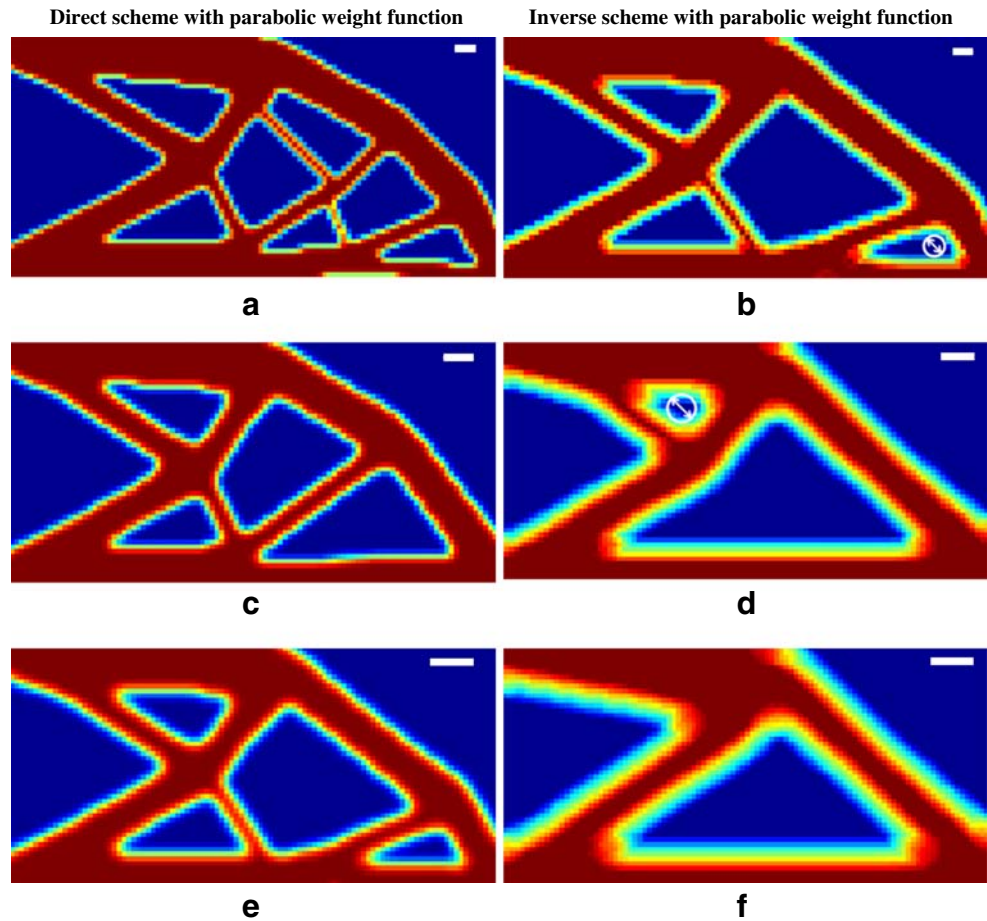


Fig. 11 Topology of the cantilever beam obtained by the inverse parabolic projection: **a** mesh discretization 100×50 and $r_{\text{inv}} = 2$ elements, **b** mesh discretization 200×100 and $r_{\text{inv}} = 4$ elements.

Note: the *white bar at the top right* illustrates the length-scale of the projection ($d = 2r_{\text{inv}}$), which spans eight elements

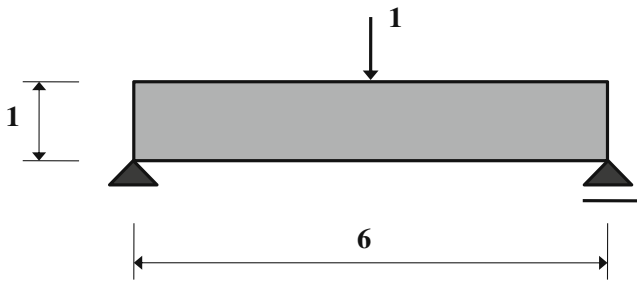


Fig. 12 MBB beam

stiffness matrix (also dependent on the design variables \mathbf{y}); f is the specified maximum volume fraction of the extended design (domain consisting of structural material); and V_0 is the volume of the design domain.

Continuation is applied to the penalization factor p of (12) using the relative change of compliance to guide the continuation criterion (e.g. if relative change in compliance between consecutive iterations is less than 2% then increment p by unity). Moreover, convergence of the topology optimization is considered satisfactory when the relative change of the norm of the design variable vector between consecutive iterations is less than a specified value (e.g. 1%).

The sensitivities with respect to the densities used in the FE analysis are evaluated using the standard adjoint method (see Bendsøe and Sigmund 2003):

$$\frac{\partial C}{\partial \rho^e} = -\mathbf{U}^T \frac{\partial \mathbf{K}}{\partial \rho^e} \mathbf{U} = -p (\rho^e)^{p-1} \mathbf{U}_e^T \frac{\partial \mathbf{K}_s^e}{\partial \rho^e} \mathbf{U}_e \quad (14)$$

Here \mathbf{U}_e is the displacement vector of element e ; and \mathbf{K}_s^e is the stiffness matrix of element e considering solid material. The design parameters adopted are the nodal densities \mathbf{y} , which are projected. The sensitivity with respect to the design variable y_k is, therefore, evaluated using the chain rule:

$$\frac{\partial C}{\partial y_k} = \sum_{e \in S_k} \frac{\partial C}{\partial \rho^e} \frac{\partial \rho^e}{\partial y_k} \quad (15)$$

The set S_k denotes the elements whose projection region Ω_w^e or Ω_{inv}^e include node k . For instance, by means of the direct projection (see (2)):

$$\frac{\partial \rho^e}{\partial y_k} = \frac{w(\mathbf{x}_k - \mathbf{x}^e)}{\sum_{j \in S_w^e} w(\mathbf{x}_j - \mathbf{x}^e)} \quad (16)$$

and by means of the inverse projection function (see (6)):

$$\frac{\partial \rho^e}{\partial y_k} = \frac{w_{inv}(\mathbf{x}_k - \mathbf{x}^e)}{\sum_{j \in S_{inv}^e} w_{inv}(\mathbf{x}_j - \mathbf{x}^e)} \quad (17)$$

An important feature regarding the implementation is the procedure to identify the nodes that influence the volume fraction of element e in the direct and in the inverse schemes. Search procedures are expensive, especially for fine meshes and large values of either r_{min} or r_{inv} . As the set of nodes lying in the regions Ω_w^e and Ω_{inv}^e are the same for all the steps of the optimization process, these search procedures are performed only once at the beginning of the algorithm. Figure 6 shows a flowchart of the single phase computational procedure.

The present numerical implementation employs uniform meshes, which avoid favoring parts of the design domain. This procedure is suitable for topology optimization modeling because it is not known, at the beginning of the procedure, where the solution is going to lie. Moreover, uniform meshes also reduce computational cost as repetition of the computation of various local stiffness matrices is eliminated by computing the element matrix for solid material at the beginning of the algorithm.

6 Projection-based two-phase topology optimization

In the flowchart presented in Fig. 6, the projection is implemented after each iteration. Another strategy is explored, which can be divided into two sequential phases (see Fig. 7):

- Phase I: In the first phase, the compliance minimization is carried out without any projection until convergence.
- Phase II: In the second phase, the chosen projection scheme is applied iteratively until a material void solution is obtained while satisfying the minimum member/size condition.

Features of the two-phase algorithm include its effectiveness (in relation to the quality of results) and the modularity of the projection-based topology optimization scheme, which can be explored in other problems such as manufacturing constraints. In order to obtain higher efficiency of the two-phase algorithm, the convergence criterion (e.g. in terms of the change of the design variables) could be looser in Phase I and tighter in Phase II. This and other aspects associated to the

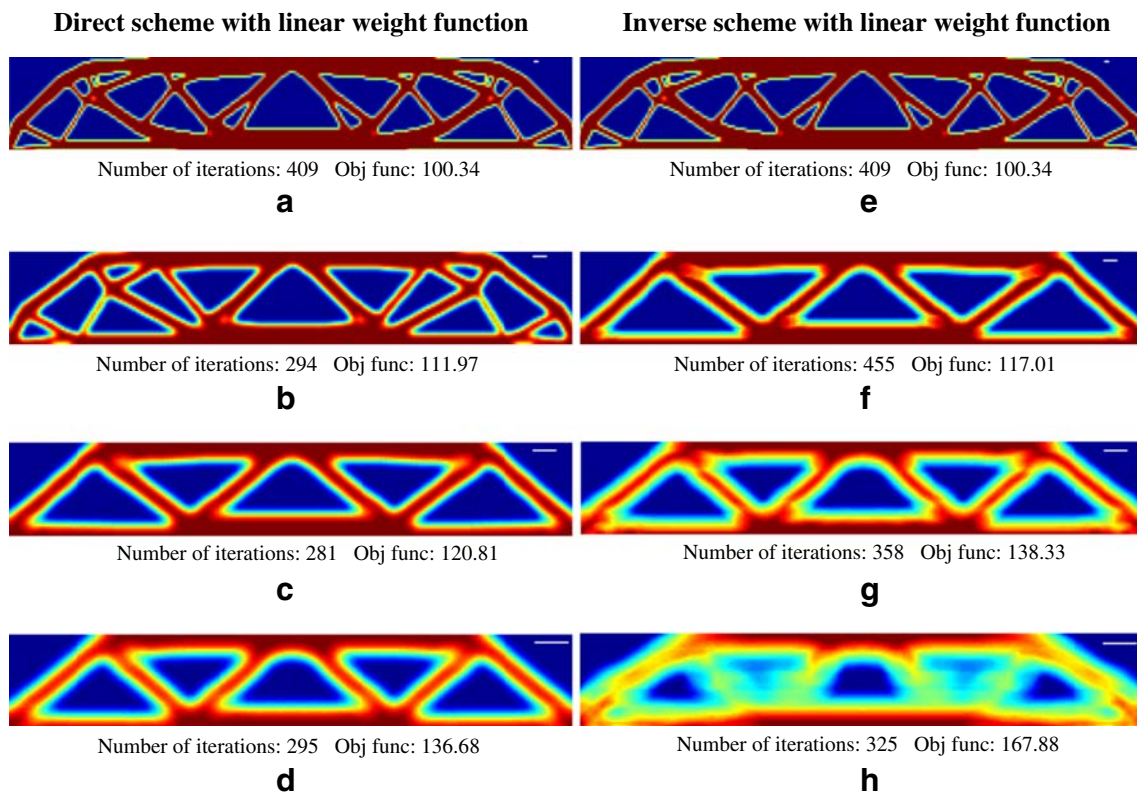


Fig. 13 Topology of the MBB beam obtained using the inverse projection scheme with linear weight function and mesh discretization 240×40 elements: **a** $r_{\min} = 1$ element, **b** $r_{\min} = 3$ elements, **c** $r_{\min} = 5$ elements, **d** $r_{\min} = 7$ elements, **e** $r_{\min} = 1$

element, **f** $r_{\min} = 3$ elements, **g** $r_{\min} = 5$ elements, **h** $r_{\min} = 7$ elements. Note: the white bar at the top right illustrates the length-scale of the projection ($d = 2r$)

computational performance of the two-phase algorithm are topics of future research.

7 Results

This section explores the projection schemes and presents numerical results for the direct, inverse, and combined schemes. The results are verified using a cantilever beam and a MBB-beam. Recall that the length scale of the direct projection scheme is $d_{\min} = 2r_{\min}$ (see Fig. 2b and c), and the length scale of the inverse projection scheme is $d_{\text{inv}} = 2r_{\text{inv}}$ (see Fig. 3b and c). For the sake of simplicity of notation, hereafter the length scale of either projection is referred as d .

All the problems are solved using four-node quadrilateral elements, and the prescribed volume of the structure is 50% of the domain volume Ω . Continuation is applied to the penalization factor of the SIMP model varying p from 1.0 to 5.0 stepping 1.0. Convergence of the topology optimization is considered satisfactory when the relative change of the norm of the design

variable vector between consecutive iterations is less than 1%). The Poisson's ratio is $\nu = 0.25$ and the Young's modulus $E = 1$. Consistent units are employed.

7.1 Inverse and direct projections

The cantilever beam problem shown in Fig. 8 is solved using both projection schemes, *i.e.* direct and inverse. The extended domain Ω is fixed along the left edge with aspect ratio of 2/1 and unit width. A point load $P = -1$ is applied to the lower left free corner of the beam.

Figure 9 shows the results obtained with both the direct and the inverse projection schemes using the linear weight functions (3) and (7), respectively. The mesh is discretized with 100×50 elements. For comparison purposes, the radius of both projections (direct and inverse) is equal to 2.0. Comparing Fig. 9a and b, one verifies the tendency of the inverse projection to coalesce the holes.

Figure 10 explores the parabolic projection and illustrates the influence of the projection area in the

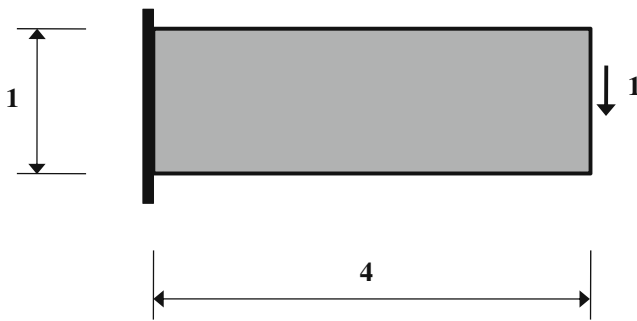


Fig. 14 Second cantilever beam

solution. Thus, the weight functions (4) and (8) are employed with varying projection radius for each scheme (direct and inverse, respectively). The mesh is discretized with 100×50 elements, and the projection radii are selected to be equal to 2, 3 and 4 elements. As expected, Fig. 10b, d and f illustrate the tendency of the inverse projection to coalesce the holes (consistent with the previous example of Fig. 9). The white bar represents $2 r_{\min}$ in Fig. 10a, c and e or $2 r_{\text{inv}}$ in Fig. 10b, d and f. The white circles in Fig. 10b and d illustrate the

regions whose sizes are closer to the minimum specified hole size ($d = 2r$).

A comparison among the linear projection results of Fig. 9a and b with those of the parabolic projection presented in Fig. 10a and b reveal some interesting results. While the direct project leads to similar topologies (Figs. 9a and 10a), the inverse projection leads to slightly different topologies (Figs. 9b and 10b). Thus while the direct projection seems to indicate nearly the same local minimum, the inverse projection does not. These results seem to indicate that the inverse projection results are more sensitive to the actual projection function adopted (linear, quadratic, etc) than the direct projection.

To address the issue of mesh dependency for the inverse projection scheme, a mesh discretized with 200×100 elements and $r_{\text{inv}} = 4.0$ elements was employed. As expected, the results displayed in Fig. 11a and b are qualitatively similar.

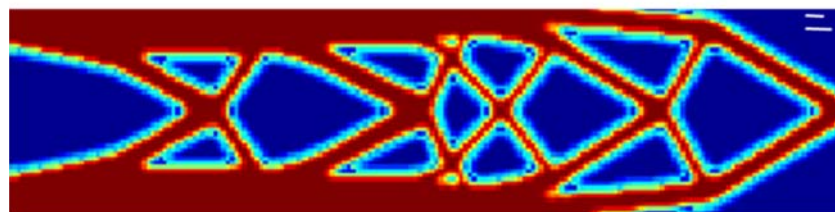
The MBB-beam problem of Fig. 12 (aspect ratio 6:1) is solved using the linear projection with both direct and inverse schemes. Due to the symmetry of the problem, only half of the beam is considered. The extended

Fig. 15 Topology of the cantilever beam obtained using the inverse projection scheme with linear weight function and mesh discretization 200×50 elements: **a** inverse projection scheme, $c_v = 0.0$ **b** combined scheme, $c_v = 0.6$ **c** direct projection scheme, $c_v = 1.0$. Note: the white bar at the top right illustrates the length-scale of the projection ($d = 2r$). The combined scheme employs both length scales



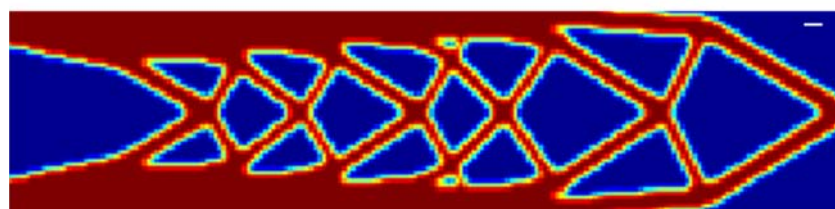
Number of iterations: 547 Objective function: 449.45

a



Number of iterations: 835 Objective function: 393.34

b



Number of iterations: 842 Objective function: 397.04

c

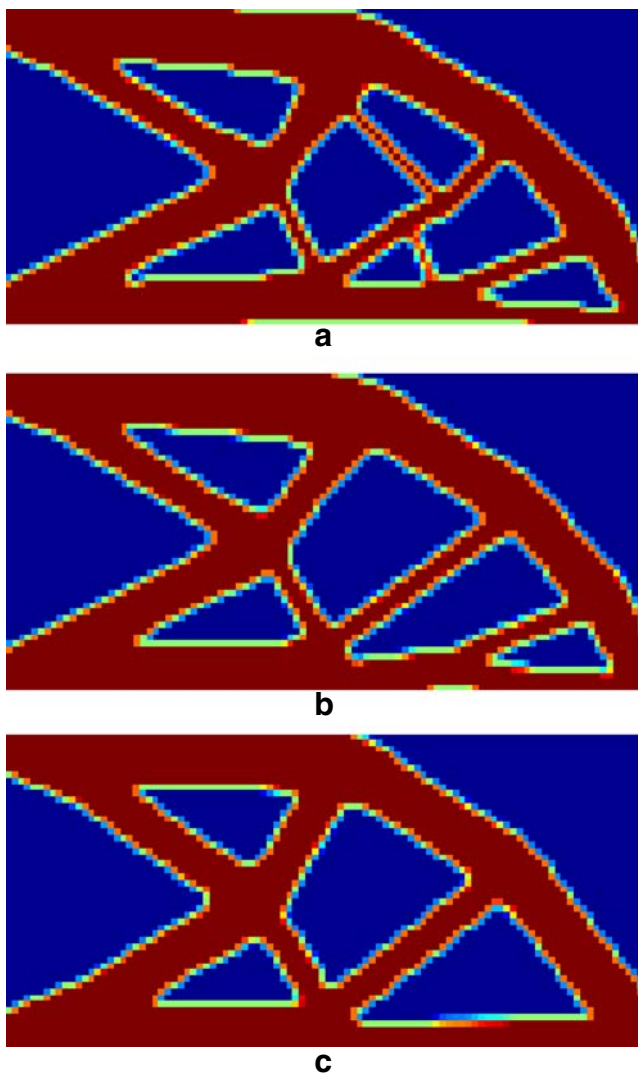


Fig. 16 Two-phase topology optimization using mesh discretization of 100×50 elements: **a** layout at the end of Phase I (no projection scheme), **b** final layout using the direct projection scheme in Phase II ($r_{\min} = 2.0$), **c** final layout using the inverse projection scheme in Phase II ($r_{\text{inv}} = 3.0$)

domain Ω is fixed along the left edge and has a length of 120 elements, height of 40 elements, and unit width. A point load $P = -1$ is applied midpoint on the top of the beam.

Table 1 Compliance results for the one-phase algorithm and for the two-phase algorithm

Projection scheme	One-phase algorithm	Two-phase algorithm	
Direct projection	78.13	End of Phase I	75.95
		First iteration of Phase II	79.04
		End of Phase II	78.86
Inverse projection	93.04	End of Phase I	75.95
		First iteration of Phase II	132.35
		End of Phase II	100.04

Figure 13 shows the results for both direct and inverse schemes with linear weight function, assuming values of r_{\min} and of r_{inv} from 1.0 to 7.0. The white bar represents $2 r_{\min}$ in Fig. 13a through d, and $2 r_{\text{inv}}$ in Fig. 13e through h. In both schemes, a “degeneration” of the solution can be observed as r_{\min} or r_{inv} increases, which occurs due to the weighted average procedure. Here the word “degeneration” refers to loss of definition of the actual structural topology. The earlier degeneration of the solution in the inverse scheme is caused by the nature of the weighted average, which benefits the densities of more distant nodes when evaluating element densities. As expected, results obtained with the parabolic weight factors are similar to the ones presented in Fig. 13, and thus are not shown here.

Moreover, when one plots the densities directly from the design variables, y_j , a picture with nearly sharp interfaces is obtained, even for higher values of the projection radius. Meanwhile, pictures displaying projected densities, ρ^e , show regions with intermediate densities for relatively high values of the projection radius. In this paper, only the projected densities are plotted.

7.2 Combined scheme

The cantilever beam problem of Fig. 14 is solved using both projection schemes, *i.e.* direct and inverse, and parabolic weight function, together with the formulation presented in Section 4. The parabolic weight functions are applied. The extended domain Ω is fixed along the left edge and has length of 200 elements, height of 50 elements, and unit width. A point load $P = -1$ is applied midway down the free right end of the beam. The penalization factor η of (10) is constant and equal to 5.0.

For the combination of the schemes, the radius of the direct projection r_{\min} is 2.0 and the radius of the inverse projection r_{inv} is 3.0. Figure 15 shows the results of the combination of the projection schemes for different change factors c_c . The projection was carried out after each iteration. The testing limit $c_c = 0.0$ (Fig. 15a) implies that $c_v^e \geq c_c$ always and, therefore, only the

inverse projection scheme is used. The testing limit $c_c = 1.0$ (Fig. 15c) implies that $c_v^e \geq c_c$ for all elements and, therefore, only the direct projection scheme is used. Intermediate values of c_c establish a competition between the two schemes, as shown in Fig. 15b. The bar line represents $2r_{\min}$ in Fig. 15a and $2r_{\text{inv}}$ in Fig. 15c. In Fig. 15b the upper white line represents $2r_{\min}$ and the lower $2r_{\text{inv}}$.

7.3 Two-phase topology optimization

In all the previous examples, the projection was implemented after each iteration of the optimization process (according to Section 5). However, in the present example, associated to Fig. 8 and with results given in Fig. 16, the two-phase strategy of Section 6 is explored according to the flowchart of Fig. 7. Figure 16a shows the layout at the end of the Phase I, which was carried out without any projection scheme. In this figure, thin structural members and small holes can be identified. The Phase II is carried out for two different instances using the linear weight function iteratively until final convergence. For the first instance, Fig. 16b presents the final layout satisfying the minimum member size condition (direct projection). For the second instance, Fig. 16c presents the final layout satisfying the minimum hole size condition (inverse projection). Table 1 presents compliance results at the end of the first phase, and at the beginning and at the end of the second phase. Results of the correspondent single phase procedures are also presented. This example illustrates the flexibility of the two-phase solution.

8 Conclusions

The inverse projection scheme developed in this paper is a simple and effective technique for void distribution control in topology optimization. Several numerical examples demonstrate the features and feasibility of the projection-based techniques presented.

The computational implementation is based on a unified approach involving mesh-independent projection techniques. Within this approach, two topology optimization implementations have been developed: one in which the projection (either inverse or direct) is employed at each iteration; and the other in which a two-phase scheme is explored. In the first phase, compliance minimization is carried out without any projection until convergence. In the second phase, the selected projection scheme (either direct or inverse) is applied iteratively until a solution is achieved.

This work offers room for further extensions. For instance, the inverse projection has been combined with a direct projection to control two distinct manufacturing features: minimum member size and minimum hole size. However, an improved and robust strategy to combine both the direct and the inverse schemes is still needed. Moreover, the present work can be extended naturally to three-dimensional problems involving three-dimensional projections. The work is also promising to be used in conjunction with manufacturing constraints such as symmetry, extrusion and machining.

Acknowledgements SRMA acknowledges the Brazilian agency CAPES for the support provided during her Sabbatical at the University of Illinois at Urbana-Champaign (UIUC) through project number 3516/06-7. GHP acknowledges FAPESP for awarding him a Visiting Scientist position during his Sabbatical at the University of São Paulo (USP) through project number 2008/5070-0. ECNS thanks the Brazilian agencies FAPESP (project number 06/57805-7) and CNPq, and the UIUC for inviting him as a Visiting Professor during the Summer/2007. We gratefully acknowledge the USA NSF through the project CMS#0303492 (Inter-Americas Collaboration in Materials Research and Education, PI Prof. W. Soboyejo, Princeton University). Finally, we acknowledge the anonymous reviewers for insightful comments which contributed to improve this paper substantially.

References

- Bendsøe MP (1989) Optimal shape design as a material distribution problem. *Struct Optim* 1(4):193–202
- Bendsøe MP, Sigmund O (2003) *Topology optimization: theory, methods and applications*. Springer, New York
- Borrvall T, Petersson J (2001) Topology optimization using regularized intermediate density control. *Comput Methods Appl Mech Eng* 190(37):4911–4928
- Bourdin B (2001) Filters in topology optimization. *Int J Numer Methods Eng* 50(9):2143–2158
- Carbonari RC, Silva ECN, Paulino GH (2007) Topology optimization design of functionally graded bimorph-type piezoelectric actuators. *Smart Mater Struc* 16(6):2605–2620
- Carbonari RC, Silva ECN, Paulino GH (2009) Multi-actuated functionally graded piezoelectric micro-tools design: a multi-physics topology optimization approach. *Int J Numer Methods Eng*. doi:10.1002/nme.2403
- Chang K-H, Tang P-S (2001) Integration of design and manufacturing for structural shape optimization. *Adv Eng Softw* 32(7):555–567
- Guest JK (2009) Imposing maximum length scale in topology optimization. *Struct Multidisc Optim*. doi:10.1007/s00158-008-0250-7
- Guest JK, Prévost JH, Belytschko T (2004) Achieving minimum length scale in topology optimization using nodal design variables and projection functions. *Int J Numer Methods Eng* 61(2):238–254
- Guo X, Gu YX (2004) A new density-stiffness interpolation scheme for topology optimization of continuum structures. *Eng Comput* 21(1):9–22

- Ishii K, Aomura S (2004) Topology optimization for the extruded three dimensional structure with constant cross section. *JSME Int J, Series A*, 47(2):198–206
- Matsui K, Terada K (2004) Continuous approximation for material distribution for topology optimization. *Int J Numer Methods Eng* 59(14):1925–1944
- Nitsopoulos I, Lauber B (2007) Overview on optimization methods, FE-DESIGN GmbH, TOSCA Structure. ANSA and META International Congress, June 14–15, 2002. <http://www.fe-design.com>
- Rozvany GIN (2001a) Topology optimization in structural mechanics. Editorial. *Struct Multidisc Optim* 21(2):89
- Rozvany GIN (2001b) Aims, scope, methods, history and unified terminology of computer-aided topology optimization in structural mechanics. *Struct Multidisc Optim* 21(2):90–108
- Sigmund O (1997) On the design of compliant mechanisms using topology optimization. *Mechan Struct Mach* 25(4):493–524
- Sigmund O (2001) Design of multiphysics actuators using topology optimization—part II: two-material structures. *Comput Methods Appl Mech Eng* 190(49–50):6605–6627
- Sigmund O (2007) Morphology-based black and white filters for topology optimization. *Struct Multidisc Optim* 33(4–5):401–424
- Wang MY, Wang S (2005) Bilateral filtering for structural topology optimization. *Int J Numer Methods Eng* 63(13):1911–1938
- Zhou M, Rozvany GIN (1991) The COC algorithm, part II: topological, geometry and generalized shape optimization. *Comput Methods Appl Mech Eng* 89(1):197–224
- Zhou M, Shyy YK, Thomas HL (2001) Checkerboard and minimum member size control in topology optimization. *Struct Multidisc Optim* 21(2):152–158
- Zuo K-T, Chen L-P, Zhang Y-Q, Yang J (2006) Manufacturing- and machining-based topology optimization. *Int J Adv Manuf Technol* 27(5–6):531–536